

Black Hole Formation in the Lower Mass Gap through Mergers and Accretion in AGN Disks

Y. Yang¹, V. Gayathri¹, I. Bartos¹, Z. Haiman², M. Safarzadeh³, and H. Tagawa⁴
Department of Physics, University of Florida, Gainesville, FL 32611-8440, USA; imrebartos@ufl.edu
Department of Astronomy, Columbia University, New York, NY, 10027, USA
Center for Astrophysics | Harvard & Smithsonian, 60 Garden Street, Cambridge, MA, USA
Astronomical Institute, Graduate School of Science, Tohoku University, Aoba, Sendai 980-8578, Japan
Received 2020 July 9; revised 2020 September 14; accepted 2020 September 16; published 2020 October 1

Abstract

The heaviest neutron stars and lightest black holes expected to be produced by stellar evolution leave the mass range $2.2\,M_\odot \lesssim m \lesssim 5\,M_\odot$ largely unpopulated. Objects found in this so-called *lower mass gap* likely originate from a distinct astrophysical process. Such an object, with mass $2.6\,M_\odot$ was recently detected in the binary merger GW190814 through gravitational waves by LIGO/Virgo. Here we show that black holes in the mass gap are naturally assembled through mergers and accretion in active galactic nucleus (AGN) disks, and can subsequently participate in additional mergers. We compute the properties of AGN-assisted mergers involving neutron stars and black holes, accounting for accretion. We find that mergers in which one of the objects is in the lower mass gap represent up to 4% of AGN-assisted mergers detectable by LIGO/Virgo. The lighter object of GW190814, with mass $2.6\,M_\odot$, could have grown in an AGN disk through accretion. We find that the unexpectedly high total mass of $3.4\,M_\odot$ observed in the neutron star merger GW190425 may also be due to accretion in an AGN disk.

Unified Astronomy Thesaurus concepts: Gravitational waves (678); Astrophysical black holes (98); Neutron stars (1108)

1. Introduction

The rapidly growing number of gravitational-wave discoveries by LIGO and Virgo have brought about several surprises (Aasi et al. 2015; Acernese et al. 2015; Abbott et al. 2019). Surprises included the unexpectedly high mass of some of the black holes, suggesting that they may have been formed through hierarchical mergers (Tagawa et al. 2020b; Yang et al. 2019a; Gayathri et al. 2020; Gerosa et al. 2020; Kimball et al. 2020; Safarzadeh et al. 2020).

More recently, two gravitational-wave detections uncovered objects with unexpected masses in the few-solar-mass range. First, neutron star merger GW190425 featured a total mass of $\sim 3.4 \, M_{\odot}$ (Abbott et al. 2020). This is substantially higher than expected from Galactic binary neutron star systems that have a total mass of \approx 2.66 \pm 0.13 (see the gray histogram in Figure 1; see also Özel et al. 2012). Second, in the binary merger GW190814, one of the observed objects had a mass of 2.6 M_{\odot} . This mass is higher than the maximum mass of nonrotating neutron stars ($\approx 2.2 M_{\odot}$; Margalit & Metzger 2017), and falls in the so-called *lower mass gap* of $\sim 2.2 - 5 M_{\odot}$ where objects are not expected from standard stellar evolution. Possible alternative supernova explosion scenarios that could populate the lower mass gap are being investigated; however, these models currently have difficulty explaining the overall binary merger rate observed by LIGO/Virgo (Zevin et al. 2020).

Other than problems with our current understanding of stellar evolution, two processes can result in objects in the $\sim 2.2-5~M_{\odot}$ range: (1) the merger of neutron stars and (2) accretion. For (1) to be relevant, neutron star mergers can occur in dense stellar environments, such as galactic centers, where the merger remnant can encounter another compact object, resulting in a binary merger that can be detected through gravitational waves (Gupta et al. 2020). Alternatively, hierarchical quadruple systems can also result in the merger of

two neutron stars and the consecutive merger of the remnant with a black hole. The second merger can be triggered either by Kozai–Lidov oscillations due to the fourth object in the system (Hamers & Safarzadeh 2020) or enhanced interaction due to a recoil kick in the wake of the merger (Fragione et al. 2020). For (2) to be relevant, accretion must be distinct from the one observed in X-ray binaries, which is not high enough to substantially increase neutron star masses (Ozel & Freire 2016; Safarzadeh & Loeb 2020).

Active galactic nuclei (AGNs) represent an environment where both hierarchical neutron star mergers and significant accretion can naturally occur. AGNs harbor a large population of neutron stars and black holes within the innermost parsec around a central supermassive black hole (SMBH; Hopman & Alexander 2006; O'Leary et al. 2009; Bartos et al. 2013; Hailey et al. 2018). These neutron stars and black holes interact with the dense accretion disk around the supermassive black hole, resulting in the orbital alignment of some of these objects and the disk (Bartos et al. 2017). Once aligned, the neutron stars and black holes can migrate within the disk, resulting in their merger either in migration traps (Bellovary et al. 2016) or at radii with a high rate of interaction with stars and compact objects outside the disk (Tagawa et al. 2020a, 2020b).

AGNs have been proposed to assist stellar-mass black hole mergers (Bartos et al. 2017; Stone et al. 2017; McKernan et al. 2018, 2019; Yang et al. 2019b, 2020). They have been proposed as a site for hierarchical black hole mergers, and several of LIGO/Virgo's binary sources were shown to be consistent with a hierarchical-AGN origin (Tagawa et al. 2020b; Yang et al. 2019a; Gayathri et al. 2020). The possibility that neutron stars can also merge in AGN disks has been proposed by McKernan et al. (2020), while the role of accretion on black hole spins in AGNs was studied by Yi et al. (2018).

In this Letter we investigate the properties of compact binary mergers in AGNs, for the first time taking into account both the

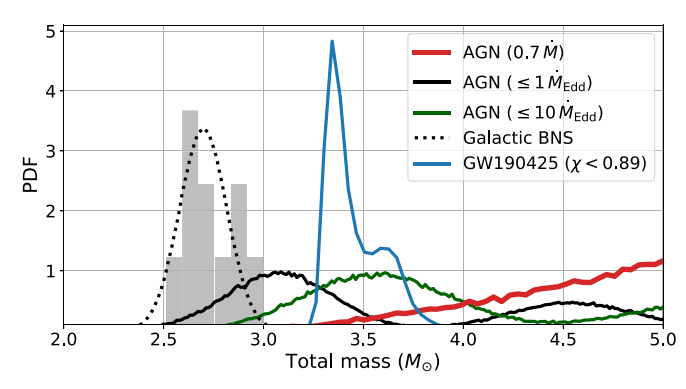


Figure 1. Probability density of total mass in compact binary mergers in AGNs, assuming a maximum accretion rate of $1\dot{M}_{Edd}$ (red) and $10\dot{M}_{Edd}$ (black), below a total mass of 5 M_{\odot} . Also shown are the total mass probability density of GW190425 (blue; assuming a uniform spin prior $\chi < 0.89$; Abbott et al. 2020), and the distribution of observed Galactic binary neutron star systems (gray).

effects of hierarchical mergers and accretion. This combination is important to quantitatively probe the properties of objects in the lower mass gap, which we focus on here. We consider whether binaries GW190425 and GW190814 observed through gravitational waves could have been produced in AGNs.

2. Method

2.1. Black Holes and Neutron Stars in the Galactic Center

We postulated that the total number of neutron stars is $f_{\rm NS:BH}=10$ times the total number of stellar-mass black holes in the broader region around the galactic nucleus unaffected by mass segregation (Hopman & Alexander 2006; Alexander & Hopman 2009). Below we discuss how our results depend on this ratio. The total mass of the black hole population is 1.6% of the stellar mass in the innermost parsec of galactic centers, i.e., about twice the SMBH's mass (Miralda-Escudé & Gould 2000). We adopted an initial mass function $dN/dm \propto m^{-2.35}$ for black holes, where m is the black hole mass. We took $5 M_{\odot}$ and $50 M_{\odot}$ as the bounds of the black hole initial mass function.

For neutron stars, we considered the mass distribution of $1.49 \pm 0.19 \, M_{\odot}$ observed for small spin period pulsars and neutron stars with high-mass companions (Ozel & Freire 2016). This mass distribution is likely near the birth masses of neutron stars that do not reside in binary neutron star systems. Given the comparable number of neutron star observations with neutron star and high-mass companions, and the fact that the latter have a much shorter lifetime due to the lifetime of the companions, this high-mass companion population is likely representative for the neutron star population as a whole. Both initial neutron stars and black holes were assumed to be spinless. This assumption does not meaningfully affect the resulting mass distribution.

Once a neutron star exceeded $2.2\,M_\odot$ due to accretion or merger, we considered it to become a black hole (Margalit & Metzger 2017). The mass at which gravitational collapse occurs depends on the neutron star's spin (Most et al. 2020); however, this limit does not substantially affect our results below.

We took into account the mass segregation in the spatial distributions of black holes and neutron stars, which are functions of the orbits semimajor axis (Gondán et al. 2018;

Alexander & Hopman 2009):

$$\frac{dn_{\rm bh}}{da} \propto a^{-3/2 - 0.5M_{\rm bh}/M_{\rm max}},\tag{1}$$

$$\frac{dn_{\rm ns}}{da} \propto a^{-3/2},\tag{2}$$

where a is the semimajor axes of the object's orbit around the SMBH, and $M_{\rm max}=50~M_{\odot}$. The higher-mass black holes typically are closer to the SMBH and neutron stars are farther away. We assumed that the maximal semimajor axis is the radius of influence of the SMBH (Bartos et al. 2017). This radius of influence is taken to be $R_{\rm inf}=1.2M_6^{1/2}$ pc based on the M- σ relation (Gültekin et al. 2009), where $M_6=M_{\bullet}/10^6M_{\odot}$ with M_{\bullet} being the SMBH mass.

2.2. The AGN disk

Following Bartos et al. (2017), we adopted a geometrically thin, optically thick, radiatively efficient, steady-state accretion disk expected in AGNs. We used a viscosity parameter $\alpha = 0.3$ and a radiation efficiency $\epsilon = 0.1$.

Observations indicate that the SMBH accretion rate for AGNs from Seyfert galaxies to bright quasars varies between $\dot{m}=\dot{M}_{\bullet}/\dot{M}_{\bullet,\rm Edd}=10^{-3}-1$ (Woo & Urry 2002), where $\dot{M}_{\rm Edd}=L_{\rm Edd}/\epsilon\,c^2$ is the Eddington rate and $L_{\rm Edd}$ is the Eddington luminosity. In our models the merger rate only changes by less than an order of magnitude between these two extreme values (see Figure 5 in Yang et al. 2019b). For simplicity, we therefore adopted the single value $\dot{m}=0.1$ and the abundance of Seyfert galaxies to be representative, for the purpose of estimating the global merger rate.

2.3. Orbital Alignment

Black holes and neutron stars orbiting the central supermassive black hole will periodically cross the AGN disk. During these crossings, black holes and neutron stars will interact with the disk, resulting in the decrease of their velocity in the direction perpendicular to the disk plane due to momentum exchange. This deceleration will eventually result in the alignment of some of the black holes' and neutron stars' orbits with the AGN disk plane.

We simulated the process of orbital alignment following the method of Yang et al. (2019b) by simulating the orbital evolution of 10^5 black holes and neutron stars. The initial orbits of these objects had an eccentricity drawn randomly from an n(e) = 2e probability density. We assumed that interactions with the disk only take place within a radius of $R_{\rm disk} = 0.1 M_6^{1/2}$ pc, beyond which they may become inhomogeneous (Haiman et al. 2009). Upon each crossing the black holes and neutron stars gravitationally capture some of the gas in the disk due to Bondi–Hoyle–Lyttleton accretion:

$$\Delta M_{\rm cross} = \Delta v t_{\rm cross} r_{\rm BHI}^2 \pi \Sigma / (2H), \tag{3}$$

where $r_{\rm BHL} \equiv 2GM_{\rm bh}/(\Delta v^2 + c_s^2)$ is the objects' Bondi–Hoyle–Lyttleton radius, Σ and H are the surface density and scale height of the AGN disk respectively, $t_{\rm cross} \equiv 2H/v_z$ is the crossing time, v_z is the z component of the object's velocity, and Δv is the relative velocity between the gas and the object upon crossing. This mass capture assumes that accretion only

occurs during the crossing time, i.e., the objects do not "drag" any matter with them that can later be accreted.

2.4. Accretion

To take into account that not all captured gas may accrete onto the compact object, we considered three accretion efficiency models. These models are intended to cover the large uncertainty relating to whether radiation feedback suppresses the accretion rate. In our models, the accretion rate onto the compact objects can exceed $\dot{M}_{\rm Edd}$ (i.e., the Eddington rate for the compact-object binary). A common assumption in the literature on BH accretion has been that radiation imposes $\dot{M}_{\rm Edd}$ as an upper limit, since radiation pressure would otherwise exceed the gravitational force. We therefore also adopt this as one of our models. However, this assumption is known to be unreliable. While AGNs generally appear to obey the Eddington limit on the luminosity, there are examples of both stellar-mass BHs and supermassive BHs that are believed to accrete at super-Eddington rates. The former include, e.g., SS 433 (e.g., Okuda 2002) and the so-called ultraluminous X-ray sources (e.g., Kawashima et al. 2012; King et al. 2017, and references therein), while the latter include so-called narrow-line Seyfert-1 galaxies (e.g., Collin & Kawaguchi 2004; Du et al. 2014, and references therein). In order to allow super-Eddington rates consistent with these observations, we adopt a second model, in which we increase the cap to $10M_{\rm Edd}$. Finally, on the theory side, it has long been argued that $\dot{M}_{\rm Edd}$ can be exceeded, even in spherical symmetry, because photons in the inner regions are trapped and advected inward with the flow (Begelman 1979). At present, modeling the accretion, over the large range of spatial scales (from the Bondi radius to the Schwarzschild radius) in realistic 3D simulations with radiative transfer is not feasible. However, modeling the accretion flows in the innermost regions around BHs, in the highly super-Eddington accretion regime, state-of-the-art numerical 3D radiation magnetohydrodynamics (MHD) simulations have found that 70% of the infalling mass is accreted, and the remaining 30% is ejected in an outflow (Jiang et al. 2019). We therefore adopt this as our fiducial model. Throughout, we adopt $\epsilon = 0.1$ as the radiation efficiency. We assumed that accretion occurs during each disk crossing and a subsequent period equal to the fallback time $r_{\rm BHL}/\Delta v$ within the radius of gravitational capture (although in practice the latter is small).

Below we adopt a fiducial SMBH mass of $M_{\bullet} = 10^6 M_{\odot}$, but note that our results only weakly depend on M_{\bullet} (Yang et al. 2019b).

2.5. Migration and Merger

Neutron stars and stellar-mass black holes are assumed to drift from their original locations inward once they have been aligned with the AGN disk (Tagawa et al. 2020a). The type I timescale for migration due to Lindblad and corotation resonance is (Tanaka et al. 2002; Paardekooper et al. 2010; Baruteau et al. 2011)

$$t_{\rm I} = \frac{1}{2f_{\rm min}} \frac{M_{\bullet}}{M_{\rm bh}} \frac{M_{\bullet}}{\Sigma r^2} \left(\frac{H}{r}\right)^2 \Omega^{-1}. \tag{4}$$

Here, $f_{\rm mig}$ is a dimensionless factor and Ω is the Keplerian angular velocity of an orbit with radius r. However, a gap will open around the object that moves in the disk if the gravitational torque exerted by the object exceeds the viscous

torque of gas; thus, the object will experience type II migration due to the torque from the gas around the gap boundary. The migration timescale for a massive migrator is given by (Duffell et al. 2014; Fung et al. 2014; Kanagawa et al. 2015, 2018)

$$t_{\rm I/II} = (1 + 0.04K)t_{\rm I},$$
 (5)

where $K = (M_{\rm bh}/M_{\bullet})^2 (H/r)^{-5} \alpha^{-1}$ and α is the viscosity parameter. The migration speed of the objects in the AGN disk is $dr/dt = -r/t_{\rm I/II}$ (Tagawa et al. 2020b). This migration speed accounts for both type I and type II migrations within the disk.

During the migration of black holes and neutron stars within the AGN disk, we assumed that their accretion is limited due to radiation produced during accretion. As our fiducial model, we assumed that 70% of the infalling matter is accreted onto the compact object (Jiang et al. 2019). To understand the role of accretion we further investigated limits at 1 and 10 times the Eddington accretion rate. While accretion also occurs during orbital alignment when the black holes and neutron stars cross the disk, due to the much higher relative velocities there, limits on accretion are relevant only at this migration phase. We adopted $f_{\rm mig}=2$ and $\alpha=0.1$ as a set of fiducial parameters in our numerical simulations.

If more than one object ends up in the AGN disk, we expect that they merge hierarchically as they migrate within the disk (Yang et al. 2019a). We assumed that the numbers of neutron stars and black holes that move into the disk follow independent Poisson distributions. We evaluated the mass and spin distributions of the remnants of binary black hole (BBH) mergers adopting the methods described in Barausse et al. (2012) and Hofmann et al. (2016). We computed the mass and spin distributions of the remnants of neutron star-black hole mergers following Zappa et al. (2019)⁵:

$$M_{\rm f} = C_{\rm BHNS}(1 - E_{\rm rad}(\eta, \hat{S}, \Delta \chi))M, \tag{6}$$

$$E_{\rm rad}(\eta, \, \hat{S}, \, \Delta \chi) = E_{\rm rad}(\eta, \, \hat{S}) + \Delta E_{\rm rad}(\eta, \, \hat{S}, \, \Delta \chi),$$
 (7)

$$E_{\text{rad}}(\eta, \, \hat{S}) = E_{\text{rad}}(\eta, \, 0)R(\hat{S}), \tag{8}$$

$$E_{\text{rad}}(\eta, 0) = \sum_{i=1}^{4} a_i \eta^i,$$
 (9)

$$R(\hat{S}) = \frac{1 + \sum_{i=1}^{3} b_i \hat{S}^i}{1 - b_5 \hat{S}},\tag{10}$$

$$b_{i} = b_{i0} \sum_{j=0}^{2} f_{ij} \eta^{j}, \tag{11}$$

$$\Delta E_{\text{rad}}(\eta, \, \hat{S}, \, \Delta \chi) = A_1(\eta) \Delta \chi + A_2(\eta) \Delta \chi^2 + A_3(\eta) \hat{S} \Delta \chi, \tag{12}$$

$$A_1(\eta) = d_{10}\sqrt{1 - 4\eta}\eta^2(d_{11}\eta + 1),\tag{13}$$

$$A_2(\eta) = d_{20}\eta^3,\tag{14}$$

$$A_3(\eta) = d_{30}\sqrt{1 - 4\eta}\,\eta(d_{31}\eta + 1),\tag{15}$$

$$C_{\text{BHNS}} = \begin{cases} 1\tilde{C} > 1 \text{ or } \chi_1 < -0.5\\ \text{or } \chi_1 < 0, \, \eta < 0.188,\\ \tilde{C} \text{ Otherwise} \end{cases}$$
 (16)

https://git.tpi.uni-jena.de/core/bhnsremnant

Table 1
The Coefficients in the Equations to Evaluate the Final Mass of the Remnant of the BH–NS Merger

			8		
$\overline{a_1}$	$1 - \frac{2\sqrt{2}}{3}$	f ₁₀	1.700455	d ₁₀	-0.122820
a_2	0.563538	f_{11}	14.393239	d_{11}	-3.499874
a_3	-0.866168	f_{20}	3.80711	d_{20}	0.014200
a_4	3.181942	f_{21}	0.0	d_{30}	-0.018737
b_{10}	-0.076946	f_{30}	25.999565	d_{31}	-5.183073
b_{20}	-0.046657	f_{31}	-232.257528		
b_{30}	-0.024309	f_{50}	1.552929		
b ₅₀	0.63876	f ₅₁	-0.842799		
p ₀₁₁	-0.001834	p ₁₁₁	2.3387×10^{-7}	p ₂₁₁	-0.02007
p ₀₁₂	0.002392	p ₁₁₂	-8.2809×10^{-7}	p ₂₁₂	0.1320
p ₀₂₁	0.004294	p ₁₂₁	-1.6432×10^{-6}	p ₂₂₁	0.06508
p ₀₂₂	0.009798	p ₁₂₂	8.0834×10^{-6}	p ₂₂₂	-0.1428

Note. $f_{i2} = 16 - 16f_{i0} - 4f_{i1}$.

$$\tilde{C} = \frac{1 + p_0 \Lambda + p_1 \Lambda^2}{(1 + p_2^2 \Lambda)^4},\tag{17}$$

$$p_{i} = p_{i1}\eta + p_{i2}\eta^{2}, \tag{18}$$

$$p_{ii} = p_{ii1} \Delta \chi + p_{ii2}, \tag{19}$$

where $M=m_1+m_2$, $\eta=m_1m_2/M^2$, $\hat{S}=(m1^2\chi_1+m_2^2\chi_2)/(m_1^2+m_2^2)$, and $\Delta\chi=\chi_1-\chi_2$. $m_{1,2}$ and $\chi_{1,2}$ are the mass and dimensionless spin of the two objects, respectively. Λ is the tidal polarizability of neutron stars. Table 1 shows the coefficients above.

The equations to compute the final spin have a similar form as the equations above but have different coefficients. Hence, we only list the distinct parts of the two sets of equations and give the coefficient in Table 2.

$$\chi_{\rm f} = C'_{\rm BHNS}(L_{\rm orb}(\eta, \hat{S}, \Delta \chi) + \chi_1 + \chi_2), \tag{20}$$

$$L_{\text{orb}}(\eta, \, \hat{S}, \, \Delta \chi) = L_{\text{orb}}(\eta, \, 0) + D(\hat{S}) + \Delta L_{\text{orb}}(\eta, \, \hat{S}, \, \Delta \chi), \tag{21}$$

$$L_{\text{orb}}(\eta, 0) = \frac{\sum_{i=1}^{3} a_i \eta^i}{1 + a_5 \eta},$$
 (22)

$$D(\hat{S}) = \frac{\sum_{i=1}^{3} b_i \hat{S}^i}{1 - b_5 \hat{S}},\tag{23}$$

$$b_{i} = b_{i0} \sum_{i=0}^{3} f_{ij} \eta^{j}, \tag{24}$$

$$\Delta L_{\text{orb}}(\eta, \, \hat{S}, \, \Delta \chi) = A_1(\eta) \Delta \chi + A_2(\eta) \Delta \chi^2 + A_3(\eta) \hat{S} \Delta \chi.$$
 (25)

We calculated the mass and spin distributions of the remnants of binary neutron star mergers following Zappa et al. (2018) and Bernuzzi et al. (2014).

$$M_{\rm f} = (1 - E_{\rm fin} \eta) M, \tag{26}$$

$$\chi_{\rm f} = (j_0 + j_1 E_{\rm fin} + j_2 E_{\rm fin}^2) \eta, \tag{27}$$

$$E_{\rm fin} = E_{\rm mrg} + E_{\rm pm},\tag{28}$$

Table 2
The Coefficients in the Equations to Evaluate the Final Spin of the Remnant of the BH–NS Merger

tile bn-N5 Weiger							
$\overline{a_1}$	$2\sqrt{3}$	f ₁₁	4.411042	d ₁₀	0.276280		
a_2	19.91807	f_{12}	0.364218	d_{11}	11.561985		
a_3	-12.22732	f_{21}	8.887933	d_{20}	-0.059758		
a_5	7.18860	f_{22}	-40.353598	d_{30}	2.729690		
b_{10}	-0.194103	f_{31}	23.927104	d_{31}	-3.388285		
b_{20}	0.066176	f_{32}	-178.781394				
b_{30}	0.0059532	f_{50}	1.898166				
b ₅₀	0.481635	f ₅₁	-5.556957				
p ₀₁₁	-0.005442	p ₁₁₁	-8.5684×10^{-7}	p ₂₁₁	-0.03042		
p_{012}	0.007912	p ₁₁₂	-2.8173×10^{-6}	p ₂₁₂	0.2549		
p_{021}	0.02334	p ₁₂₁	6.6129×10^{-6}	p ₂₂₁	0.14755		
p_{022}	0.02478	p_{122}	4.2898×10^{-5}	p_{222}	-0.4279		

Note. $f_{i3} = 64 - 64f_{i0} - 16f_{i1} - 4f_{i2}$, $f_{10} = f_{20} = f_{30} = f_{52} = 0$.

Table 3
The Coefficients in the Equations to Evaluate the Final Mass and Spin of the Remnant of the BNS Merger

$\overline{\mathbf{j}_0}$	4.39507	c_1	0.050917	p ₁	2.443586
j_1	-17.21173	c_2	6.44074×10^{-5}	p_2	-0.0189288
j_2	38.54988	c_3	0.095325	b_1	-5.126437×10^{-5}
E_0	0.12	c_4	2.64027×10^{-4}	b_2	0.038079
κ_0	0.0012				

$$E_{\text{mrg}} = E_0 \frac{1 + c_1 \kappa + c_2 \kappa^2}{1 + c_3 \kappa + c_4 \kappa^2},$$
 (29)

$$\kappa = \kappa_2^{\mathrm{T}} + \kappa_0 (1 - 4\eta), \tag{30}$$

$$\kappa_2^{\mathrm{T}} = \frac{3q^4}{(1+q)^5} \Lambda_1 + \frac{3q^{-4}}{(1+q^{-1})^5} \Lambda_2,$$
(31)

$$E_{\text{pm}} = \begin{cases} 0.018 & \kappa_2^{\text{T}} < 63\\ 0.059 & 63 \leqslant \kappa_2^{\text{T}} < 73\\ p_1 \kappa_2^{\text{T} - \frac{7}{10}} + p_2 & 73 \leqslant \kappa_2^{\text{T}} < 475.9 \\ b_1 \kappa_2^{\text{T}} + b_2 & 475.9 \leqslant \kappa_2^{\text{T}} < 742.8\\ 0 & \text{Otherwise} \end{cases}$$
(32)

where $q = m_2/m_1$, $M = m_1 + m_2$, $\eta = m_1 m_2/M^2$, $m_{1,2}$, and $\Lambda_{1,2}$ are the mass and tidal polarizability of the two neutron stars, respectively. The coefficients are displayed in Table 3.

We then simulated 10⁶ samples to characterize the distributions of binaries' masses and effective spins.⁷

2.6. Relative Rate of Binary Merger Types

We found that the expected frequencies of coalescence for the three binary types under total number $N \geqslant 2$ of neutron stars and black holes are $R_{\rm BNS}(N) = p^2$, $R_{\rm NSBH}(N) = Np - 2p^2$, and $R_{\rm BBH}(N) = N - 1 - Np + p^2$, where $p = \lambda_{\rm NS}/(\lambda_{\rm NS} + \lambda_{\rm BH})$ is the mean fraction of neutron stars in the AGN disk. It is not hard to show that N has a Poisson distribution with a mean value $\lambda = \lambda_{\rm NS} + \lambda_{\rm BH}$; thus, the

binary and $\vec{S}_{1,2}$ are the spin parameters of the two compact stars in the binary.

⁶ https://git.tpi.uni-jena.de/core/bns_lum

 $^{7 \}quad \chi_{\text{eff}} \equiv \frac{c}{GM} \left(\frac{\vec{S}_1}{m_1} + \frac{\vec{s}_2}{m_2} \right) \cdot \frac{\vec{L}}{|\vec{L}|}, \text{ where } M = m_1 + m_2 \text{ is the total mass of the}$

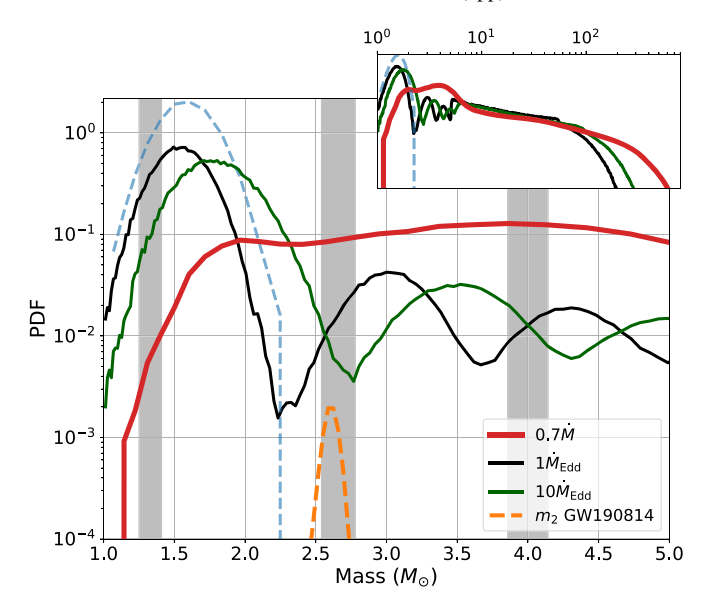


Figure 2. The mass distributions of compact objects undergoing mergers in AGN disks. The main figure shows the distribution in the lower mass gap, while the inset shows the distribution for a wider range of masses. We show results for three accretion models: when 70% of the infalling matter is accreted onto the compact object (red; Jiang et al. 2019), accretion is limited to $1\dot{M}_{\rm Edd}$ (black) and $10\dot{M}_{\rm Edd}$ (green). The multipeaked structure shows different generations in hierarchical mergers. For comparison, we show the distribution of the lighter component mass m_2 of binary merger GW190814 (orange; Abbott et al. 2020), as well as our initial mass function for neutron stars (blue dashed, main figure) and black holes (blue dashed, inset). We also show the expected mass ranges of neutron stars and hierarchically merged neutron stars the Galactic mass distribution found in binary neutron star systems, neglecting mass loss or accretion (vertical gray bands).

overall expected frequencies of mergers for one AGN are

$$\langle R_{\rm BNS} \rangle = p^2 P_{\rm N \geqslant 2},$$
 (33)

$$\langle R_{\text{NSBH}} \rangle = (1 - e^{-\lambda}) \lambda p - 2p^2 P_{\text{N} \geqslant 2},$$
 (34)

$$\langle R_{\rm BBH} \rangle = (1 - e^{-\lambda})\lambda(1 - p) + (p^2 - 1)P_{\rm N \geqslant 2},$$
 (35)

where $P_{N\geqslant 2}=1-(1+\lambda)e^{-\lambda}$ is the probability of $N\geqslant 2$.

For an SMBH with mass $10^6 M_{\odot}$, we found that the average number of black holes whose orbits are aligned with the AGN disk within the AGN lifetime ($\tau_{\rm AGN} \sim 10^7 \ \rm yr$) is 3, whereas that of neutron stars is about 19. These numbers depend on our assumption of $f_{\rm NS:BH}$, which we took to be 10. If we adopt the Salpeter initial mass function and assume that 20–140 M_{\odot} stars form BHs as in Tagawa et al. (2020b), and 8–20 M_{\odot} stars form NSs, $f_{\rm NS:BH} \simeq 2.5$, which would correspond to an average number of 5 for neutron star alignments, where we kept the black hole number density fixed.

3. Results

The mass distributions we obtained through Monte Carlo simulations are shown in Figure 2, both for the $1\dot{M}_{\rm Edd}$ and $10\dot{M}_{\rm Edd}$ limits. The distribution of the total mass of binaries is shown in Figure 1. We found that the mass distribution at low masses substantially deviates from a simple power law, with clear peaks and troughs. This oscillatory distribution is the consequence of hierarchical neutron star mergers. The width of each period in these bands is determined by the initial mass distribution of neutron stars and accretion.

We computed the merger rate of binary neutron stars, neutron star-black hole, and binary black hole systems in a

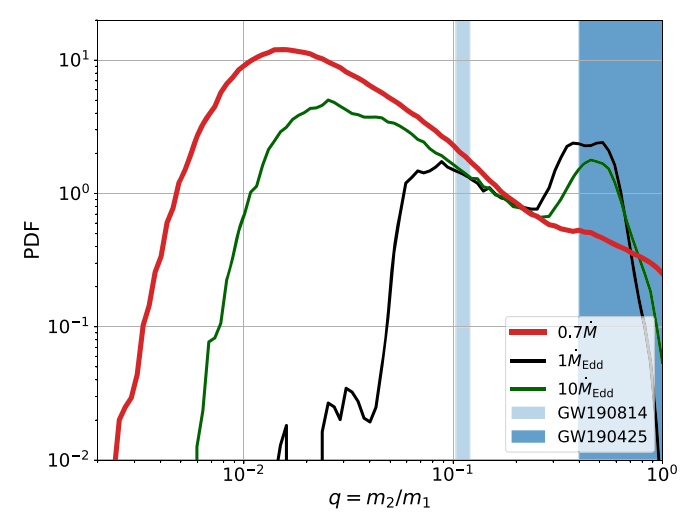


Figure 3. The mass ratio distributions of compact objects undergoing mergers in AGN disks. The plot shows the distribution of mass ratio around the lower mass gap. We show results for three accretion models: when 70% of the infalling matter is accreted onto the compact object (red; Jiang et al. 2019) and accretion is limited to $1\dot{M}_{\rm Edd}$ (black) and to $10\dot{M}_{\rm Edd}$ (green). For comparison, we show the mass ratio limit for binary mergers GW190814 (light blue; Abbott et al. 2020) and GW190425 (blue; assuming a uniform spin prior $\chi < 0.89$; Abbott et al. 2020).

single AGN. We adopted a number density of $n_{\text{Seyfert}} = 0.018$ Mpc⁻³ for Seyfert galaxies (Hao et al. 2005) and converted the single-AGN merger rate to the local merger rate density using $R_{\text{cosmic}} = n_{\text{Seyfert}} R_{\text{single}}$. This conversion is justified as R_{single} only weakly depends on the SMBH mass in the galaxy. The obtained rates are listed in Table 4.

We see that the merger rates of binary neutron star, neutron star-black hole, and binary black hole systems are comparable in AGNs. However, since the sensitivity of LIGO/Virgo strongly depends on mass, the relative detection rates of the different types will be markedly different from their merger rates. We computed the fractional detection rates of the different merger types considering LIGO/Virgo's design sensitivity. The relative fractions we obtained are listed in Table 4. We see that the detection rate is dominated by binary black holes. Mergers in which one of the objects is in the lower mass gap will represent $\sim 1\%$ of detections, i.e., their detection is expected once the total number of detected events is $\mathcal{O}(100)$.

These above results are based on $f_{\rm NS:BH}=10$. To assess the dependence of our results on this number we considered here an alternative $f_{\rm NS:BH}=2.5$ assumed by Tagawa et al. (2020b). This reduction of the neutron star number density would decrease the fractional rate of binaries with a neutron star component by approximately a factor of 4. This change also affects the fraction of events with a component in the mass gap. For example for our fiducial model of $0.7\dot{M}$ accretion, only about 1% of LIGO/Virgo's detections would be expected to have a component in the lower mass gap.

4. Conclusions

We investigated the effect of hierarchical mergers and accretion in AGN disks on the mass distribution of neutron stars and black holes, mainly focusing on the lower mass gap, $2.2-5~M_{\odot}$. Our conclusions are as follows:

 Neutron star-black hole and binary black hole mergers are expected in AGNs at comparable rates, while binary

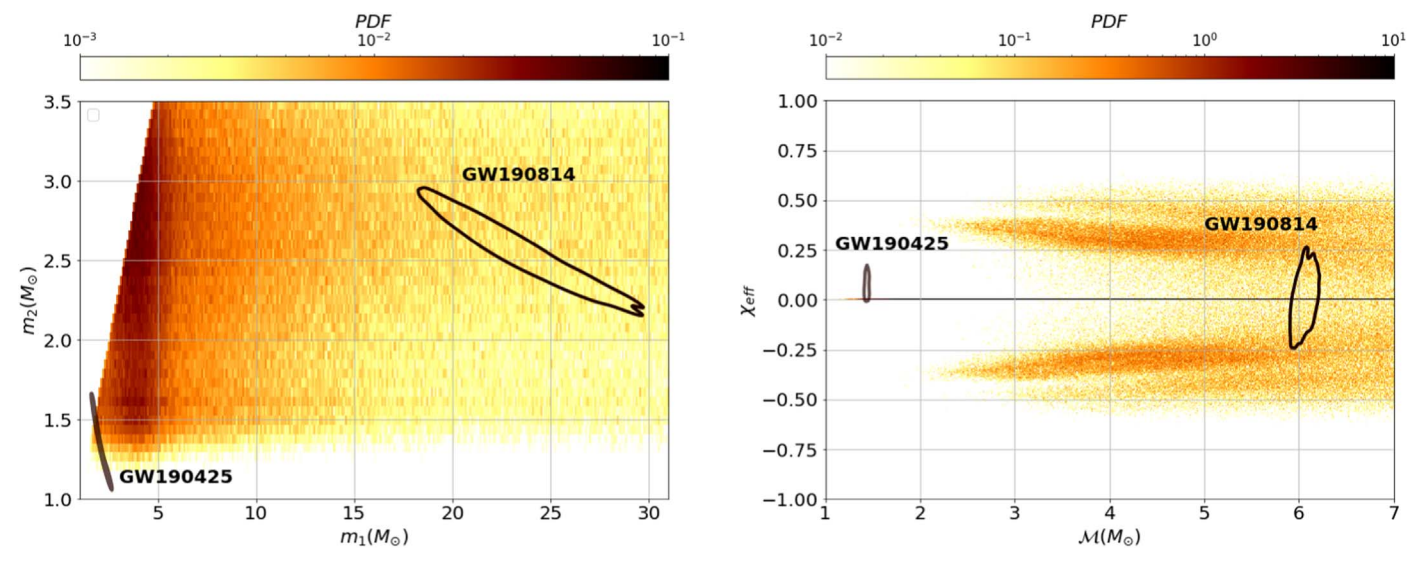


Figure 4. Mass and spin probability densities of AGN-assisted mergers. We show the probability density on the $m_1 - m_2$ plane (left) and on the chirp mass—effective spin plane (right). We also show the reconstructed distributions for GW190425 and GW190814. Note that for low chirp masses $\mathcal{M} \lesssim 2$, we have $\chi_{\text{eff}} = 0$ as we assume that neutron stars have negligible spin, i.e., the probability density has nonnegligible support for GW190425.

 ${\bf Table~4}\\ {\bf Merger~Rate~and~Detection~Fraction~for~Different~Types~of~Compact~Binary~Mergers}$

Type	Merger Rate		Merger Rate Density		Det. Fraction [%]				
1) PC	$[10^{-7} \text{yr}^{-1}]$			[Gpc ⁻³ yr ⁻¹]					
	0.7 <i>M</i>	1 M _{Edd}	10 M _{Edd}	$0.7\dot{M}$	1 M _{Edd}	10 M _{Edd}	0.7 <i>M</i>	1 M _{Edd}	10 M _{Edd}
BNS	0.01	0.4	0.3	0.02	0.6	0.6	0.0001	0.01	0.005
NS-BH	0.06	3.5	3.4	1.1	6.3	6.1	0.07	0.9	0.5
BBH	5.0	2.3	2.5	9.0	4.1	4.5	99.9	99.1	99.5
$2.2 M_{\odot} < M < 5 M_{\odot}$	1.7	0.7	0.8	3.1	1.2	1.5	3.9	0.5	0.4
$50 M_{\odot} < M$	1.7	2.2	3.1	3.0	3.8	5.6	76.7	52.3	76
$65 M_{\odot} < M$	1.5	1.2	2.4	2.6	2.2	4.2	60.8	26.5	57

Note. We show the merger rate in a given AGN and the merger rate density in the local universe for the three accretion models considered here. We additionally show the expected fraction of LIGO/Virgo observations for each binary type, taking into account the mass-dependent sensitive distance of LIGO/Virgo at design sensitivity. We consider binary neutron stars (BNS), neutron star-black hole systems (NS-BH), and binary black holes (BBH). An object with mass >2.2 M_{\odot} is considered a black hole. We further show these quantities separately for those binaries in which one of the masses falls into the lower mass gap (2.2 M_{\odot} < M_{\odot} or the upper mass gap (considering two lower bounds of this mass gap, 50 M_{\odot} and 65 M_{\odot}).

neutron star mergers are also expected but less often (see Table 4).

- 2. Up to 4% of AGN-assisted binary mergers observed by LIGO/Virgo will include a component in the lower mass gap. Gravitational-wave detections from AGNs will be mostly binary black holes (99%), with ≤1% contribution from neutron star–black hole mergers, and ≪1% fractional detection from binary neutron stars (see Table 4).
- Both accretion and hierarchical mergers significantly contribute to the resulting mass distribution of binary mergers in AGNs. However, most objects in the mass gap are the remnant of a merger.
- 4. The $2.6 \, M_{\odot}$ mass of the mass gap object in binary merger GW190814 (see Figure 2), as well as the binary's mass ratio (see Figure 3 and Figure 4), are consistent with having arisen in an AGN disk. An AGN origin also naturally explains the observed high mass ratio for the event, which is unlikely in field binaries (Safarzadeh & Hotokezaka 2020) and is suppressed in globular clusters due to mass segregation (Gerosa et al. 2020; Ye et al. 2020).

5. The binary neutron star merger GW190425 had a total mass consistent with the expected mass distribution in AGNs. However, the small expected detection rate of neutron star mergers in AGNs decreases the likelihood of an AGN origin.

We thank Yan-Fei Jiang, Christopher Berry, and Wenbin Lu for helpful discussions. I.B. acknowledges support from the Alfred P. Sloan Foundation and the University of Florida. Z.H. acknowledges support from NASA grant 80NSSC18K1093 and NSF grant 1715661.

ORCID iDs

I. Bartos https://orcid.org/0000-0001-5607-3637 M. Safarzadeh https://orcid.org/0000-0002-1827-7011

References

Aasi, J., Abbott, B. P., Abbott, R., et al. 2015, CQGra, 32, 074001 Abbott, B. P., Abbott, R., Abbott, T. D., et al. 2020, ApJL, 892, L3

```
Abbott, B. P., Abbott, R., Abbott, T. D., et al. 2019, PhRvX, 9, 031040
Abbott, R., Abbott, T. D., Abraham, S., et al. 2020, ApJL, 896, L44
Acernese, F., Agathos, M., Agatsuma, K., et al. 2015, CQGra, 32, 024001
Alexander, T., & Hopman, C. 2009, ApJ, 697, 1861
Barausse, E., Morozova, V., & Rezzolla, L. 2012, ApJ, 758, 63
Bartos, I., Haiman, Z., Kocsis, B., & Márka, S. 2013, PhRvL, 110, 221102
Bartos, I., Kocsis, B., Haiman, Z., & Márka, S. 2017, ApJ, 835, 165
Baruteau, C., Cuadra, J., & Lin, D. N. C. 2011, ApJ, 726, 28
Begelman, M. C. 1979, MNRAS, 187, 237
Bellovary, J. M., Mac Low, M.-M., McKernan, B., & Ford, K. E. S. 2016,
   ApJL, 819, L17
Bernuzzi, S., Nagar, A., Balmelli, S., Dietrich, T., & Ujevic, M. 2014, PhRvL,
   112, 201101
Collin, S., & Kawaguchi, T. 2004, A&A, 426, 797
Du, P., Hu, C., Lu, K.-X., et al. 2014, ApJ, 782, 45
Duffell, P. C., Haiman, Z., MacFadyen, A. I., D'Orazio, D. J., & Farris, B. D.
  2014, ApJL, 792, L10
Fragione, G., Loeb, A., & Rasio, F. A. 2020, ApJL, 895, L15
Fung, J., Shi, J.-M., & Chiang, E. 2014, ApJ, 782, 88
Gayathri, V., Bartos, I., Haiman, Z., et al. 2020, ApJL, 890, L20
Gerosa, D., Vitale, S., & Berti, E. 2020, PhRvL, 125, 101103
Gondán, L., Kocsis, B., Raffai, P., & Frei, Z. 2018, ApJ, 860, 5
Gültekin, K., Richstone, D. O., Gebhardt, K., et al. 2009, ApJ, 698, 198
Gupta, A., Gerosa, D., Arun, K. G., et al. 2020, PhRvD, 101, 103036
Hailey, C. J., Mori, K., Bauer, F. E., et al. 2018, Natur, 556, 70
Haiman, Z., Kocsis, B., & Menou, K. 2009, ApJ, 700, 1952
Hamers, A. S., & Safarzadeh, M. 2020, ApJ, 898, 99
Hao, L., Strauss, M. A., Fan, X., et al. 2005, AJ, 129, 1795
Hofmann, F., Barausse, E., & Rezzolla, L. 2016, ApJL, 825, L19
Hopman, C., & Alexander, T. 2006, ApJL, 645, L133
Jiang, Y.-F., Stone, J. M., & Davis, S. W. 2019, ApJ, 880, 67
Kanagawa, K. D., Muto, T., Tanaka, H., et al. 2015, ApJL, 806, L15
Kanagawa, K. D., Tanaka, H., & Szuszkiewicz, E. 2018, ApJ, 861, 140
Kawashima, T., Ohsuga, K., Mineshige, S., et al. 2012, ApJ, 752, 18
```

```
Kimball, C., Talbot, C., Berry, C. P. L., et al. 2020, ApJ, 900, 177
King, A., Lasota, J.-P., & Kluźniak, W. 2017, MNRAS, 468, L59
Margalit, B., & Metzger, B. D. 2017, ApJL, 850, L19
McKernan, B., Ford, K. E. S., Bartos, I., et al. 2019, ApJL, 884, L50
McKernan, B., Ford, K. E. S., Bellovary, J., et al. 2018, ApJ, 866, 66
McKernan, B., Ford, K. E. S., & O'Shaughnessy, R. 2020, arXiv:2002.00046
Miralda-Escudé, J., & Gould, A. 2000, ApJ, 545, 847
Most, E. R., Papenfort, L. J., Weih, L. R., & Rezzolla, L. 2020, arXiv:2006.
Okuda, T. 2002, PASJ, 54, 253
O'Leary, R. M., Kocsis, B., & Loeb, A. 2009, MNRAS, 395, 2127
Ozel, F., & Freire, P. 2016, ARA&A, 54, 401
Özel, F., Psaltis, D., Narayan, R., & Santos Villarreal, A. 2012, ApJ,
Paardekooper, S. J., Baruteau, C., Crida, A., & Kley, W. 2010, MNRAS,
  401, 1950
Safarzadeh, M., Hamers, A. S., Loeb, A., & Berger, E. 2020, ApJL, 888, L3
Safarzadeh, M., & Hotokezaka, K. 2020, ApJL, 897, L7
Safarzadeh, M., & Loeb, A. 2020, ApJL, 899, L15
Stone, N. C., Metzger, B. D., & Haiman, Z. 2017, MNRAS, 464, 946
Tagawa, H., Haiman, Z., Bartos, I., & Kocsis, B. 2020a, ApJ, 899, 26
Tagawa, H., Haiman, Z., & Kocsis, B. 2020b, ApJ, 898, 25
Tanaka, H., Takeuchi, T., & Ward, W. R. 2002, ApJ, 565, 1257
Woo, J.-H., & Urry, C. M. 2002, ApJ, 579, 530
Yang, Y., Bartos, I., Gayathri, V., et al. 2019a, PhRvL, 123, 181101
Yang, Y., Bartos, I., Haiman, Z., et al. 2019b, ApJ, 876, 122
Yang, Y., Bartos, I., Haiman, Z., et al. 2020, ApJ, 896, 138
Ye, C. S., Fong, W.-f., Kremer, K., et al. 2020, ApJL, 888, L10
Yi, S.-X., Cheng, K. S., & Taam, R. E. 2018, ApJL, 859, L25
Zappa, F., Bernuzzi, S., Pannarale, F., Mapelli, M., & Giacobbo, N. 2019,
       L, 123, 041102
Zappa, F., Bernuzzi, S., Radice, D., Perego, A., & Dietrich, T. 2018, PhRvL,
   120, 111101
Zevin, M., Spera, M., Berry, C. P. L., & Kalogera, V. 2020, ApJL, 899, L1
```